Inorganic Chemistry

Article

pubs.acs.org/IC

Preferential Solvation of Metastable Phases Relevant to Topological Control Within the Synthesis of Metal−Organic Frameworks

Xiaoning Yang*,† and Aurora E. Clark*,‡

†College of Chemistry and Chemical Engineering, Nanjing University of Technology, Nanjing 21009, China

‡Department of Chemistry and the Materials Science and Engineering Program, Washington State University, Pullman, Washington 99164, United States

Supporting Information

ABSTRACT: A combined density functional theory and molecular dynamics study has been used to study reactions relevant to the crystallization of a model cluster based upon the metastable phase NH_2-MOF-235(Al), which has been previously shown to be an important intermediate in the synthesis of NH_2-MIL-101(Al). The clusters studied were of the form $Al_3O(BDC)_6(DMF)_n(H_2O)_m^+$, where BDC^- = NH_2-benzenedicarboxylate and DMF = dimethylformamide (n = 1−3; m = {n − 3}). The ionic bonding interaction of the Al_3O^{7+} core with BDC^- is much stronger than that with a coordinated solvent and is independent of the bulk solvent medium (water or DMF). The exchange reactions of a coordinated solvent are predicted to be facile, and the dynamic solvent organization indicates that they are kinetically allowed because of the ability of the solvent to migrate into the cleft created by the BDC−Al_3O−BDC coordination angle. As BDC^- binds to the Al_3O^{7+} core, the solvation free energy (G_{solv}) of the cluster becomes less favorable, presumably because of the overall hydrophobicity of the cluster. These data indicate that as the crystal grows there is a balance between the energy gained by BDC^- coordination and an increasingly unfavorable G_{solv}. Ultimately, unfavorable solvation energies will inhibit the formation of quantifiable metal−organic framework (MOF) crystals unless solution-phase conditions can be used to maintain thermodynamically favorable solute−solvent interactions. Toward this end, the addition of a cosolvent is found to alter solvation of $Al_3O(BDC)_6(DMF)_3^+$ because more hydrophobic solvents (DMF, methanol, acetonitrile, and isopropyl alcohol) preferentially solvate the MOF cluster and exclude water from the immediate solvation shells. The preferential solvation is maintained even at temperatures relevant to the hydrothermal synthesis of MOFs. While all cosolvents exhibit this preferential solvation, trends do exist. Ranking the cosolvents based upon their observed ability to exclude water from the MOF cluster yields acetonitrile < DMF ∼ methanol < isopropyl alcohol. These observations are anticipated to impact the intermediate and final phases observed in MOF synthesis by creating favorable solvation environments for specific MOF topologies. This adds further insight into recent reports wherein DMF has been implicated in the reactive transformation of NH_2-MOF-235(Al) to NH_2-MOF-101(Al), suggesting that that DMF additionally plays a vital role in stabilizing the metastable NH_2-MOF-235(Al) phase early in the synthesis.

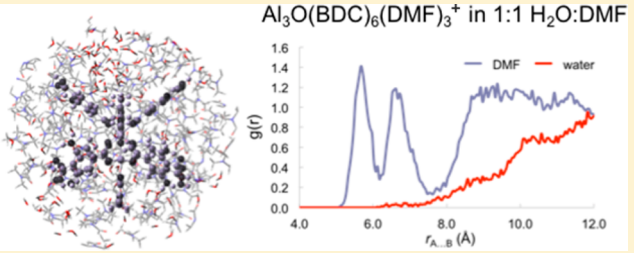

INTRODUCTION

Metal−organic frameworks (MOFs) are a class of network structures that are characterized by hybrid inorganic/organic building blocks.[1] They can possess large surface areas with high porosity, and their physical properties can be tuned by the appropriate selection of the building blocks and/or post-synthetic modifications.[2,3] These properties make MOFs promising materials in industry for separation,[4−6] storage,[7,8] catalysis,[9−11] drug delivery,[12,13] luminescence,[14] and magnetism.[15] Yet these applications are highly dependent upon a reliable and controlled large-scale synthesis.[2] While new frameworks of MOFs are reported each year, synthesis methods with scale-up in large quantities and less synthesis time must be developed.[2] One key challenge in the synthesis of MOFs is that the fundamental crystallization mechanism, its kinetic and thermodynamic driving forces, has yet to be fully understood. This is one reason why new MOF topologies are often discovered by chance rather than design.[16,17] Elucidating the mechanism over multiple length and time scales will ultimately enable the rational design of next-generation MOFs with targeted designed topologies and properties.

MOF syntheses are often performed under hydrothermal conditions, where solution-phase concentrations of reagent precursors or cosolvents are manipulated to promote ligand exchange and/or crystallization.[2,16] Recent experimental studies have begun to unravel the role of the solution-phase conditions through in situ measurements of the dissolution and crystallization kinetics, either by X-ray absorption,[18] dynamic light scattering,[19] atomic force microscopy,[20] X-ray diffraction,[21] NMR,[22] of small- and wide-angle X-ray scattering (SAXS/WAXS).[23] In a recent study,[23] the synthesis of NH_2-

Received: March 25, 2014
Published: August 21, 2014

   dx.doi.org/10.1021/ic5006659 | Inorg. Chem. 2014, 53, 8930−8940

MIL-101(Al) and NH_2-MIL-53(Al) was investigated using a combined SAXS/WAXS approach, wherein it was observed that a metastable NH_2-MOF-235(Al) phase was formed. The reactivity of this intermediate was found to be modulated by the concentration of a cosolvent, dimethylformamide (DMF), in water (H_2O). Higher concentrations of DMF stabilized the crystallization of NH_2-MOF-235(Al) and led to an improved material yield of the final product, NH_2-MIL-101(Al), relative to pure H_2O. A follow-up study using in situ NMR and gas-phase density functional theory (DFT) examined potential reactions that cause transformation of the NH_2-MOF-53(Al) topology to NH_2-MIL-101(Al).[24] That data indicated that exchange of the coordinated DMF cosolvent with H_2O may stabilize the NH_2-MIL-101 topology *and* that it may act as a source of hydroxido ligands, required for transformation of NH_2-MOF-235(Al) to NH_2-MIL-101(Al) via a bimolecular reaction of DMF with $AlCl_4^-$. Other recent studies have also implicated cosolvent reactivity, specifically acetone, in the reduction of Fe^{III} to Fe^{II} in the formation of metastable MIL-45(Fe) porous iron carboxylates, which similarly transform into MIL-100(Fe).[25]

The role of cosolvents in MOF synthesis, whether it be as an active reactant, or as a means for modulating the solubility of growing MOF crystallites, will be significantly influenced by the changing dielectric constant of the solution, in addition to solvation organization and dynamics about the reactive species. For example, solvent-exchange rates may ultimately play a limiting role in the reaction kinetics in the same way that it is an upper bound to the rate of metal−ligand complexation in traditional solution phase inorganic syntheses. The solvation of growing MOF intermediate phases (or clusters) is particularly interesting, because the essential building blocks of the MOF can contain both hydrophobic and hydrophilic units. It is thus possible for complex solvation organization and dynamics to emerge as H_2O and the cosolvent seek to maximize hydrogen bonding while at the same time minimizing hydrophobic interactions. Concurrently, the dielectric constant of the solution will impact the overall solubility of MOF intermediates and, potentially, the thermodynamics of the individual solvent- and ligand-exchange reactions relevant to crystal growth and/or dissolution.

The goal of the current work is 3-fold: (1) to examine whether exchange of coordinating solvent molecules in binary solutions can influence the metal−linker binding energy within a MOF cluster that represents a stable intermediate found during crystallization; (2) to investigate whether the changing dielectric constant of binary solutions may impact solvent- and ligand-exchange thermodynamics; (3) to better understand the role of solvation upon reactivity of the cluster, particularly when that cluster has both hydrophobic and hydrophilic regions, by examining the organization and dynamics of unary and binary solvents. A combination of DFT and classical molecular dynamics (MD) has been employed, and a model system that represents the metastable NH_2-MOF-235(Al) phase described above has been utilized because this system has been well-characterized in terms of its reactivity and is representative of other metastable intermediates found during MOF synthesis. Ligand and solvent exchange, in addition to solvation dynamics, has been investigated for the clusters $Al_3O(BDC)_6(DMF)_n(H_2O)_m^+$ ($n = 1-3$; $m = \{n - 3\}$) in H_2O and DMF solvents, while $Al_3O(BDC)_6(DMF)_3^+$ has been studied in binary systems that include 1:1 mixtures of H_2O with DMF, acetonitrile (CH_3CN), methanol (MeOH), and isopropyl alcohol [$(CH_3)_2CHOH$].

COMPUTATIONAL AND SIMULATION METHODS

DFT geometry optimizations, frequency, and polarizable continuum model (PCM) calculations were performed using *Gaussian-09* (*G09*),[26] with Becke's three-parameter hybrid exchange-correlation density functional B3LYP[27,28] and the cc-pVDZ basis set[29] on all atoms. Following gas-phase optimization of $Al_3O(BDC)_6(DMF)_n(H_2O)_m^+$ ($n = 1-3$; $m = \{n - 3\}$) and $Al_3O(BDC)_5(DMF)_n(H_2O)_m^+$ ($n = 1-5$; $m = \{n - 5\}$), normal-mode analysis confirmed each cluster to be a local minimum on the potential energy surface. The Cartesian coordinates of each optimized cluster are presented in Tables S1−S10 in the Supporting Information (SI). The importance of the basis-set superposition error (BSSE), using the counterpoise correction of Bernardi,[30] was tested in the gas-phase thermodynamic values for select reactions (Table S11 in the SI) and was found to be 2−3 kcal/mol using the cc-pVDZ basis set. Thus, non-BSSE-corrected values are reported. The gas-phase electronic structure was examined using the localized orbital locator (LOL) approach, as implemented in the *Multiwfn* code,[31] while bond-order calculations were performed using the definitions of Mayer[32] and that from natural bond order (NBO) analysis[33,34] in *G09*. The solution-phase thermodynamics were studied based upon single-point calculations at the gas-phase-optimized geometries with the integral equation variant of the PCM (IEFPCM)[35] to determine solution-phase free energies in pure H_2O (dielectric constant, ε, of 78.4) and DMF ($\varepsilon = 37.2$) solvents.

Classical MD simulations used DL_POLY.[36] Cubic simulation boxes were constructed wherein the optimized DFT geometry of the MOF cluster $Al_3O(BDC)_6(DMF)_3^+$ was immersed in solvent media using *Packmole*.[37] Here, a rigid cluster should be a good approximation to the true cluster in solution because the low-energy vibrational modes (<300 cm^{-1}) consist of low-amplitude librational modes of the BDC^- and DMF groups and low-amplitude bends of the terminal $-NH_2$ functionalities (see Table S12 in the SI). While these motions may couple to the solvent dynamics, it is unlikely to be a large perturbation to the solvent organization, which is the emphasis of this study. The simulation of the cluster in pure H_2O used 5100 H_2O molecules in a 53.3^3 Å^3 box, while the simulation in pure DMF used 1000 solvent molecules in a 51.5^3 Å^3 box, and the 1:1 H_2O/DMF mixture used 1000 H_2O and 1000 DMF in a 54.7^3 Å^3 box. Other 1:1 binary solutions were studied, including simulation boxes with 3000 H_2O and 3000 MeOH (64.8^3 Å^3 box), 2000 H_2O and 2000 CH_3CN (61.7^3 Å^3 box), and 2000 H_2O with 2000 $(CH_3)_2CHOH$ (67.5^3 Å^3 box). The $AlCl_4^-$ counterion was not considered in this work because it is unlikely to be strongly associated with the monocation not only because of the low overall charge of the ions but also because of sterics at the Al_3O core and because the 1+ charge of $Al_3O(BDC)_6(DMF)_3^+$ is not localized to a single site but rather delocalized across the Al_3O^{7+} core and the coordinating and nearest-neighbor atoms of the BDC^- and DMF units. The nonbonded interactions were represented by a sum of the Coulomb and Lennard-Jones terms as eq 1

$$E_{ab} = \sum_i^a \sum_j^b \left[\frac{q_i q_j e^2}{r_{ij}} + 4\epsilon \left(\frac{\sigma_{ij}^{12}}{r_{ij}^{12}} - \frac{\sigma_{ij}^{6}}{r_{ij}^{6}} \right) \right] \quad (1)$$

where E_{ab} is the interaction energy between centers a and b. The Dreiding force field[38] was used to describe the rigid NH_2-MOF-235 cluster, which is capable of predicting the structures and dynamics of organic, biological, and main-group inorganic molecules. The atomic charges for the NH_2-MOF-235 cluster were obtained from Mulliken analysis of the DFT orbitals. H_2O was simulated using the SPC/E[39] model, and DMF was simulated using a modified OPLS-AA model,[40−42] which represents the pure liquid experimental density and heat of vaporization. The TraPPE-UA model was used to describe CH_3CN in the H_2O/$(CH_3)CN$ solution[43] and the H_2O/CH_3OH and H_2O/$(CH_3)_2CHOH$ solutions.[44] Note that these different models have fairly consistent O-atom charges within the solvent molecules,

dx.doi.org/10.1021/ic5006659 | *Inorg. Chem.* 2014, 53, 8930−8940

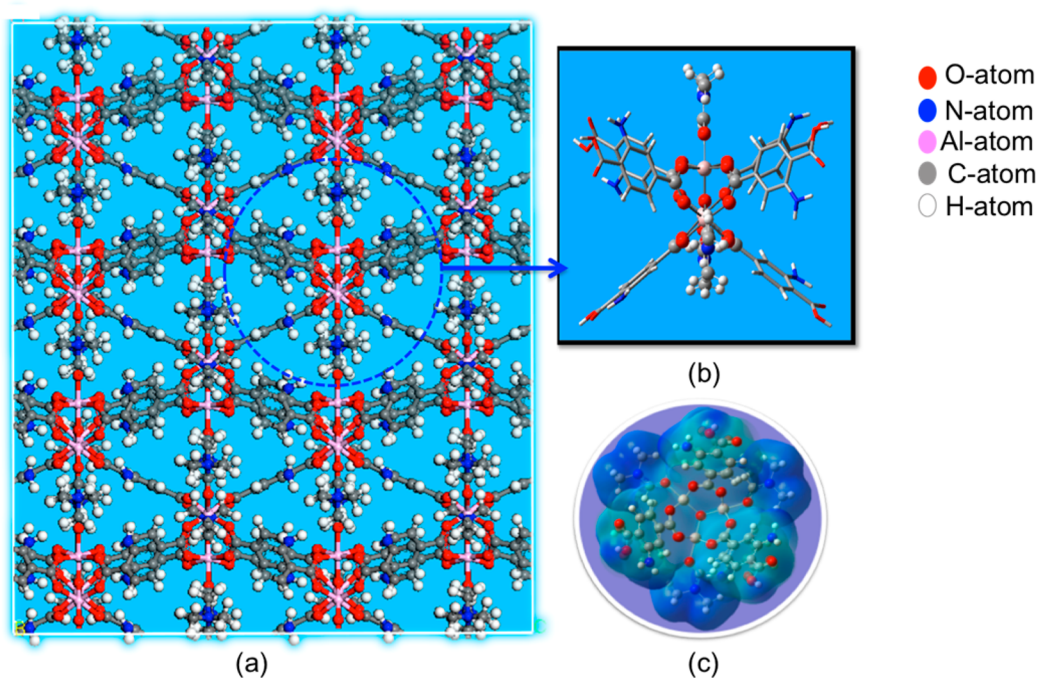

Figure 1. (a) Three-dimensional pore structure of NH_2-MOF-235. (b) B3LYP/cc-pVDZ-optimized $Al_3O(BDC)_6(DMF)_3^+$ cluster. (c) Electrostatic potential distribution of $Al_3O(BDC)_6(DMF)_3^+$. The circle in part a represents the selected cluster model.

with the H_2O O atom having a charge of 0.83−, alcoholic H atoms having a charge of 0.7−, and DMF having an O-atom charge of 0.5−. In contrast, the Mulliken-predicted charges for the BDC ligands in $Al_3O(BDC)_6(DMF)_3^+$ are somewhat smaller, 0.3− to 0.15− (Table S13 in the SI). This may impact the hydrogen-bond formation between the solvent and noncoordinated carboxylate groups of BDC^-; however, because of the presence of an intramolecular hydrogen bond between these carboxylate groups and the ortho $-NH_2$ group, the impact upon the qualitative features of solvation is likely negligible. The standard Lorentz−Berthelot (L−B) mixing rule was applied for the van der Waals (vdW) interaction of unlike particles. MD simulations were performed in the isothermal−isobaric ensemble[45,46] (NPT) at a temperature of 300 K and a pressure of 1.0 atm. The Nosé−Hoover method[47−49] was used for temperature control, and periodic boundary conditions were used in all three directions. Newton's equation of motion was integrated using the velocity Verlet algorithm[50] with a time step of 1 fs. The cutoff distance for nonbonded interaction was set as 12 Å. For each MD simulation, a total 5.0 ns run was conducted, where the first 3 ns was for equilibrium. Equilibrated simulation variables are presented in Figures S1 and S2 in the Supporting Information.

RESULTS AND DISCUSSION

Validity and Characteristics of the NH_2-MOF-235(Al) Cluster Model. No reported crystal structure coordinates are available, to our best knowledge, for the metastable NH_2-MOF-235(Al) phase, and thus the cluster model employed had its initial coordinates carved from the reported crystal structure coordinates of NH_2-MOF-235(Fe),[51] with the replacement of Fe^{III} with Al^{III}. As shown in Figure 1a, this NH_2-MOF-235 structure consists of μ_3-O-bridged trigonal secondary building units that are connected through linear NH_2-1,4-BDC^- linkers, creating a three-dimensional pore structure. Each Al atom in the Al_3O^{7+} core center has two additional unique types of Al−O linkages: one is the bond to the O atoms of the carboxylate BDC^- ligands, and the other is the bond to the O atoms of either solvating DMF or H_2O. This structure should capture the essential features of the growing NH_2-MOF-235(Al) phase and allow for a study of the solvent-accessible surfaces, relative hydrophobic and hydrophilic regions, and potential solvent- and ligand-exchange thermodynamics in solution. Table 1 lists selected bond distances and angles for the optimized clusters $Al_3O(BDC)_6(DMF)_3^+$ and $Al_3(BDC)_6(H_2O)_3^+$, with Figure 1b presenting the optimized cluster structure of $Al_3O(BDC)_6(DMF)_3^+$, in which the O-centered aluminum carboxylate trimer is included in the cluster model. The Al_3O^{7+} plane in the $Al_3O(CO_6)$ core has an Al−μ_3-O−Al angle of ∼120°, which is very similar to the structure in MOF-235(Fe).[51] While the organic structural features are nearly identical with those of MOF-235(Fe), the Al−Al separation is ∼3.2 Å, slightly lower than the distance in MOF-235(Fe).[51] It is interesting to note that the bond distance between the Al atom and O atom of DMF ($Al-O_{DMF}$) has been elongated by about 0.6 Å compared

Table 1. Selected Bond Lengths (Å), Bond Angles (deg), and Bond Orders for the NH_2-MOF-235 Clusters $Al_3O(BDC)_6(DMF)_3^+$ and $Al_3O(BDC)_6(H_2O)_3^+$, Where O_{core} is the O Atom in the Al_3O^{7+} Core[a]

atom pair	r_{Al-O} (Å)	bond order		bond angle (deg)	
		Mayer	NBO		
$Al_3O(BDC)_6(DMF)_3^+$					
$Al-O_{core}$	1.86	0.69	0.37	$Al-O_{core}-Al$	120.0
$Al-O_{BDC}$	1.94	0.60	0.33	$O_{BDC}-Al-O_{BDC}$	87.4
$Al-O_{DMF}$	2.01	0.55	0.29	$O_{core}-Al-O_{BDC}$	96.2
				$O_{core}-Al-O_{DMF}$	179.2
$Al_3O(BDC)_6(H_2O)_3^+$					
$Al-O_{core}$	1.83	0.68	0.38	$Al-O_{core}-Al$	120.0
$Al-O_{BDC}$	1.93	0.64	0.36	$O_{BDC}-Al-O_{BDC}$	87.8
$Al-O_w$	2.04	0.53	0.29	$O_{core}-Al-O_{BDC}$	97.1
				$O_{core}-Al-O_w$	178.4

[a] O_{BDC}, O_{DMF}, and O_w are the coordinating O atoms of BDC^-, DMF, and H_2O, respectively.

dx.doi.org/10.1021/ic5006659 | Inorg. Chem. 2014, 53, 8930−8940

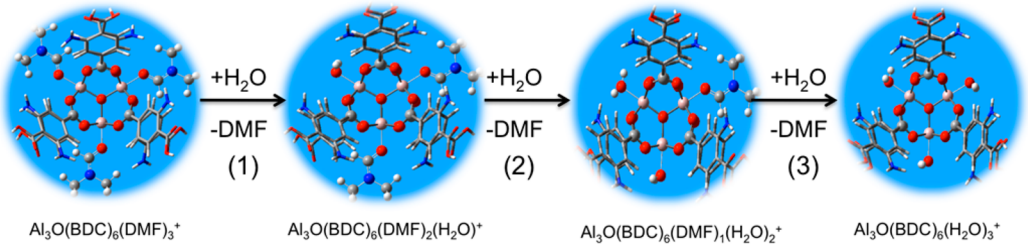

Figure 2. Illustration of exchange reactions for DMF and H_2O coordinating solvents.

with the bond length of Al−O_{BDC}. This may suggest a decrease in the bonding strength of Al−O_{DMF} compared with that of Al−O_{BDC} (vide infra).

NH_2-MOF-235 Solvent Exchange and Ligand Displacement Reactivity. It is generally believed that the metal−linker bonds in MOFs are relatively weak.[52] Extensive research has shown that H_2O molecules may easily penetrate into the porous network and participate in ligand replacement and/or hydrolysis. These observations may be due to changes in the electronic structure of the reactive MOF with the solvent because ligating solvent molecules may donate electrons to the positively charged metal core building blocks, thereby decreasing the electrostatic interaction between the metal and anionic linker. To investigate the ability of a solvent to alter MOF reactivity during the dissolution (or crystallization) process, the thermodynamics of both solvent exchange and linker dissociation have been examined with DMF and H_2O coordinating solvents.

Solvent-Exchange Reactions in Binary H_2O/DMF Solutions. DMF and H_2O molecules are characterized by a very different electronic structure; however, from an electrostatic perspective at the coordinating O atom, they are quite similar. The coordinating O atom of gas-phase DMF has a Mulliken charge of 0.24−, while the O atom of H_2O has a charge of 0.26− (see Tablse S13 and S14 in the SI). If the primary interaction between the Al_3O^{7+} core and a coordinating solvent molecule is electrostatic (e.g., ion-induced dipole), then one would expect solvent ligation by DMF and H_2O to have similar thermodynamic favorability. Solvent-exchange reactions for DMF and H_2O at the Al_3O^{7+} coordination site are illustrated in Figure 2. Beginning with the cluster $Al_3O(BDC)_6(DMF)_3^+$, it is observed that exchange of the first DMF for H_2O is mildly endergonic in the gas phase (Table 2) and in either H_2O or DMF solvents (represented by a bulk dielectric continuum). These gas-phase values are consistent with prior M06L[53,54] DFT calculations, wherein solvent exchange was examined during the transformation of NH_2-MIL-53(Al) to NH_2-MIL-101(Al).[24] They are also within the typical error of DFT calculations (nominally 5 kcal/mol), and thus at elevated temperatures, solvent exchange should be facile. To explore the role of DFT within these data, single-point calculations at the B3LYP-optimized geometry have been performed using the long-range and dispersion-corrected M06L functional.[53,54] Although the M06L reaction energies for solvent exchange, ΔE_{rxn}, are nearly double those of B3LYP, they too are under 5 kcal/mol, supporting facile solvent exchange (Table S11 in the SI). As observed in Table 1, the replacement of all coordinating DMF molecules with H_2O does not significantly alter the geometry of the MOF cluster studied. Further, the atomic charges on the BDC^- and Al_3O^{7+} core are not significantly perturbed upon solvent exchange (Tables S13 and S14 in the SI), indicating that the NH_2-MOF-235 cluster has a very similar electronic structure irrespective of the coordinating DMF or H_2O at the Al positions.

Table 2. Gas- and Solution-Phase Free Energies (ΔG_{rxn}) in kcal/mol for Reactions (1)−(3), Representing the Solvent-Exchange Reaction for the NH_2-MOF-235 Cluster

reaction	gas-phase free energy	in H_2O	in DMF
1	0.78	0.29	0.83
2	0.41	−0.89	−0.76
3	−0.45	−1.38	−1.21

$$Al_3O(BDC)_6(DMF)_3^+ + H_2O \rightarrow Al_3O(BDC)_6(DMF)_2(H_2O)^+ + DMF \quad (1)$$

$$Al_3O(BDC)_6(DMF)_2(H_2O)^+H_2O \rightarrow Al_3O(BDC)_6(DMF)(H_2O)_2^+ + DMF \quad (2)$$

$$Al_3O(BDC)_6(DMF)(H_2O)_2^+ + H_2O \rightarrow Al_3O(BDC)_6(H_2O)_3^+ + DMF \quad (3)$$

BDC Linker Replacement Reactions by Coordinating Solvents. In prior work, the metastable NH_2-MOF-235(Al) phase was observed to form in binary H_2O/DMF solutions, presumably because DMF enhanced the solubility of the BDC^- linker.[23] While this may be true, it is useful to examine how the changing coordination environment of a growing NH_2-MOF-235 cluster may be influenced by the change in the solution-phase concentrations of DMF and H_2O. Because increased DMF concentrations do enhance the growth of NH_2-MOF-235(Al), we begin by examining the strength and electronic nature of the Al_3O-BDC electronic interaction when the metal core is coordinated by DMF, as in $Al_3O(BDC)_6(DMF)_3^+$, which would be found at higher mole fractions of DMF in solution. First, the linker replacement reactions were examined, where either DMF or H_2O solvent molecules may replace BDC^-:

$$Al_3O(BDC)_6(DMF)_3^+ + DMF \rightarrow Al_3O(BDC)_5(DMF)_4^{2+} + BDC^- \quad (4)$$

$$Al_3O(BDC)_6(DMF)_3^+ + 2H_2O \rightarrow Al_3O(BDC)_5(DMF)_3(H_2O)_2^{2+} + BDC^- \quad (5)$$

The replacement reactions of BDC^- were then examined as the number of coordinating DMF molecules was decreased and the coordinating H_2O was increased, as might be expected for binary solutions with smaller mole fractions of DMF:

dx.doi.org/10.1021/ic5006659 | Inorg. Chem. 2014, 53, 8930−8940

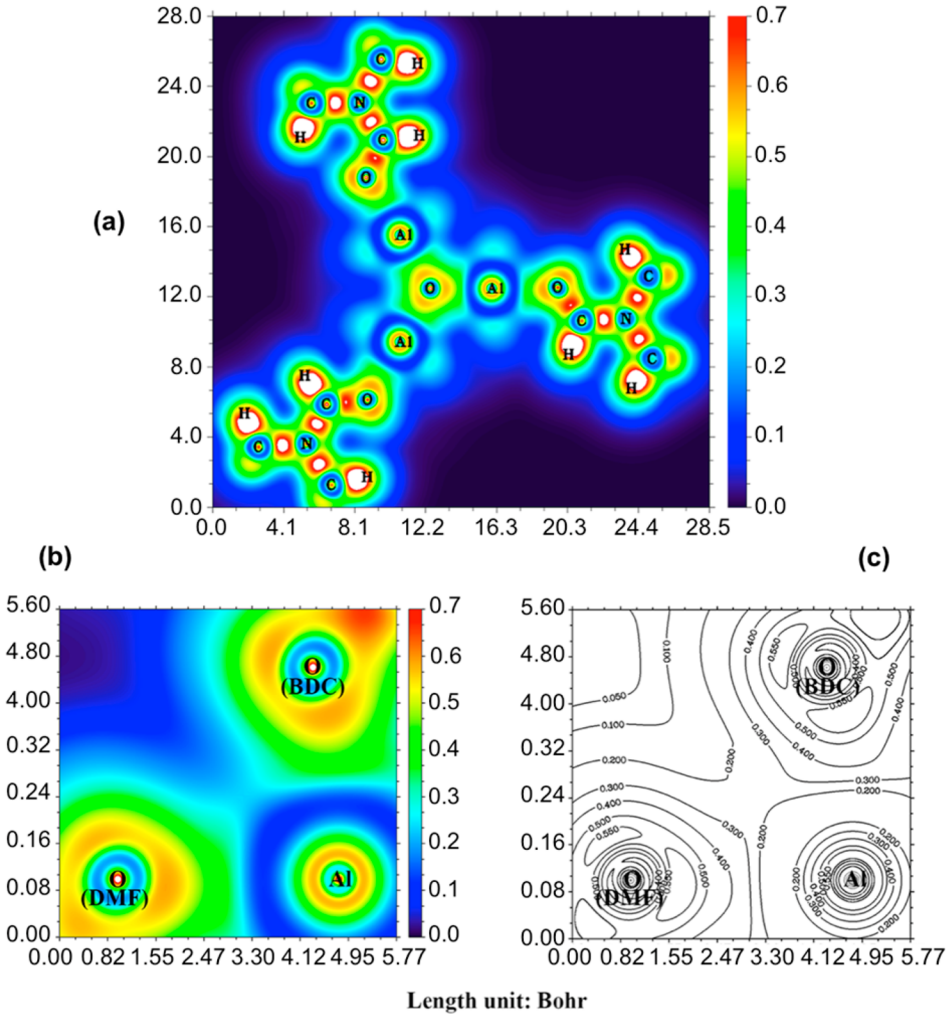

Figure 3. LOL for the NH_2-MOF-235 cluster $Al_3O(BDC)_6(DMF)_3^+$. (a) Two-dimensional filled-color maps along the Al_3O^{7+} plane. Regions with values higher than 0.7 are denoted as white. (b) LOL along the Al−O_{BDC}−O_{DMF} plane. (c) Two-dimensional isovalue LOL figure along the Al−O_{BDC}−O_{DMF} plane.

$$Al_3O(BDC)_6(DMF)_2(H_2O)^+ + 2H_2O \rightarrow Al_3O(BDC)_5(DMF)_2(H_2O)_3^{2+} + BDC^- \quad (6)$$

$$Al_3O(BDC)_6(DMF)(H_2O)_2^+ + 2H_2O \rightarrow Al_3O(BDC)_5(DMF)_2(H_2O)_4^{2+} + BDC^- \quad (7)$$

$$Al_3O(BDC)_6(H_2O)_3^+ + 2H_2O \rightarrow Al_3O(BDC)_5(H_2O)_5^{2+} + BDC^- \quad (8)$$

Replacement of BDC^- is highly unfavorable for reactions (4)−(8), and the free energies are found to be insensitive to the bulk dielectric constant of the solution. This is particularly interesting because while DMF and H_2O are miscible solvents, DMF has a dramatically reduced dielectric constant of 37.2, compared to the H_2O value of 78.4 (as implemented in the PCM of *G09*). The free energy for BDC^- replacement is significantly larger than that for the coordinating solvent exchange, indicating that the metal−linker interaction is quite strong. Analysis of the Al−O bond order between the metal−linker and metal−solvent was performed using both the Mayer and NBO methods. As can be seen in Table 1, although the Mayer bond orders are modestly larger than those from NBO, they both predict that the largest bond order is in Al−O_{core}, followed by the Al−O_{BDC} bond, and finally by the nearly equivalent Al−O_{DMF} and Al−O_w. These data are consistent with the predicted bond lengths, which systematically increase from ∼1.8 to 2.0 Å for Al−O_{core} < Al−O_{BDC} < Al−O_{DMF} ≈ Al−O_w. However, the magnitude of the bond order is <1 for both methods, indicating a predominantly ionic interaction between the Al and O atoms for BDC^-, DMF, and H_2O.

The nature of the Al−O interaction is further elucidated using the LOL, proposed by Schmider and Becke,[55] which provides electron localization information between two bonding atoms. Figure 3a presents the two-dimensional projection LOL for the Al_3O^{7+} core in the NH_2-MOF-235 cluster. No obvious electron localization between Al−O_{core} bonds is observed, whereas there is significant electron localization for the known covalent bonds (C−C, C−N, etc.). The two-dimensional LOL for the O_{DMF}−Al−O_{BDC} plane is given in Figure 3b, where a similar electronic structure is observed between the Al and coordinating O atoms of the DMF ligand or the BDC^- linker. This is in line with the basic feature of ionic bonding for all Al−O interactions in the MOF cluster. Figure 3c gives the relevant isovalue curve. From the LOL result, only a very small distinction can be found between the Al−O_{BDC}, Al−O_{DMF}, and Al−O_w covalencies, in agreement

dx.doi.org/10.1021/ic5006659 | *Inorg. Chem.* 2014, 53, 8930−8940

with the bond-order calculations (Table 1). Thus, the large endothermic reaction energy for the linker dissociation reactions is reflective of the enhanced electrostatic attraction of the negatively charged BDC^- with the formally Al^{3+} atoms.[24] It should be noted that the electrostatic interaction may change as the MOF cluster grows because of delocalization of the electron density, which is beyond the scope of the current work but may be of interest in the study of postsynthetic modification strategies.

In addition to the generally larger free energies of BDC^- replacement compared to solvent exchange, several other interesting features emerge from the data presented in Table 3.

Table 3. Gas- and Solution-Phase Free Energies (ΔG_{rxn}) in kcal/mol for Reactions (4)−(8), Representing Linker Replacement from the MOF Cluster

reaction	gas-phase free energy	in H_2O	in DMF
4	148.01	28.61	29.99
5	144.13	20.88	20.35
6	151.74	22.75	21.96
7	153.60	20.28	19.11
8	160.38	20.79	19.36

Note that reaction (4) in solution is ∼30 kcal/mol, while reactions (5)−(8) are all ∼20 kcal/mol. Thus, it is consistently more favorable for BDC^- to be replaced by H_2O than by DMF, irrespective of the coordinating solvent or dielectric constant representing the bulk solvent. Interestingly, the gas-phase ΔG_{rxn} values do not follow this trend and instead become more positive as more coordinating H_2O molecules are present [reactions (6)−(8)], indicating that the presence of coordinating H_2O does not decrease the metal−linker binding energy relative to when DMF is the coordinating solvent. Instead, the decrease in ΔG_{rxn} in the solution phase is attributable to more negative solvation free energies of the MOF cluster when BDC^- is replaced by H_2O. This is due to an increase in the electrostatic contribution to the free energy in solution caused by a larger charge buildup near the coordinating H_2O, relative to the bulkier hydrophobic BDC^- ligand. Although this observation might be dismissed as an artifact of the PCM approach, the organization of the solvent H_2O and DMF molecules, as discussed below in the MD simulation data, supports the overall hydrophobic nature of the $Al_3(BDC)_6(DMF)_3^+$ cluster, and thus a more negative free energy of solvation would be anticipated as H_2O replaces BDC^- (vide infra). When this is looked at from a crystallization perspective instead of a dissolution point of view, the net results from reactions (4)−(8) indicate that the strong electrostatic interaction between BDC^- and the Al_3O^{7+} core overcomes the energetic penalty in the solvation free energy as the hydrophobic BDC^- groups are added to the Al_3O^{7+} core within the growing NH_2-MOF-235 cluster/crystallite. This highlights the importance of including solution-phase corrections to gas-phase ab initio calculations, which have been generally ignored in prior studies. The solution-phase conditions, and the ability to tune the solvation free energy by changing solvent systems, are thus anticipated to become very important to the ability of the cluster to grow into a metastable crystalline phase. This thermodynamic and electronic structure perspective on coordinating solvent exchange and linker replacement agrees very well with the most recent experimental studies[23,56] of the transformation of NH_2-MOF-235(Al) into NH_2-MIL-101(Al) and provides added insight into the enhanced stabilization for the formation of NH_2-MOF-235(Al) in binary H_2O/DMF solvents.

Dynamic Solvent Organization in Unary and Binary Solutions. The $Al_3O(BDC)_6(DMF)_n(H_2O)_m^+$ (n = 1−3; m = "n − 3") clusters are interesting solutes because they contain both hydrophobic and hydrophilic regions. The relative hydrophobicity/hydrophilicity is evident in the electrostatic potential surface for the $Al_3O(BDC)_6(DMF)_3^+$ cluster presented Figure 1c. Sites with more negative charges, near the O atoms of the Al_3O^{7+} core and the O atoms from BDC^- and DMF, will have a higher likelihood of participating in hydrogen bonding, while the weakly positive benzene rings of the BDC^- linkers will have hydrophobic character.

The organization of H_2O about $Al_3O(BDC)_6(DMF)_3^+$ in a pure H_2O MD simulation box was first investigated through the

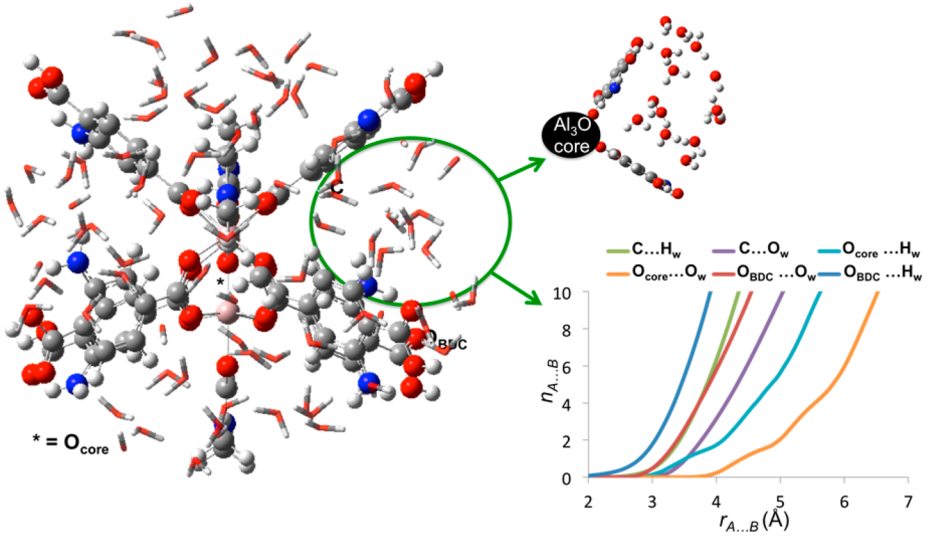

Figure 4. Representative solvent organization (within 12 Å of O_{core}) about $Al_3O(BDC)_6(DMF)_3^+$ immersed in pure H_2O. The solvation within the BDC−Al_3O−BDC cleft is inset along with key integrated RDFs between functional groups of $Al_3O(BDC)_6(DMF)_3^+$ and H_2O (O_w and H_w represent the O and H atoms of H_2O, respectively).

dx.doi.org/10.1021/ic5006659 | Inorg. Chem. 2014, 53, 8930−8940

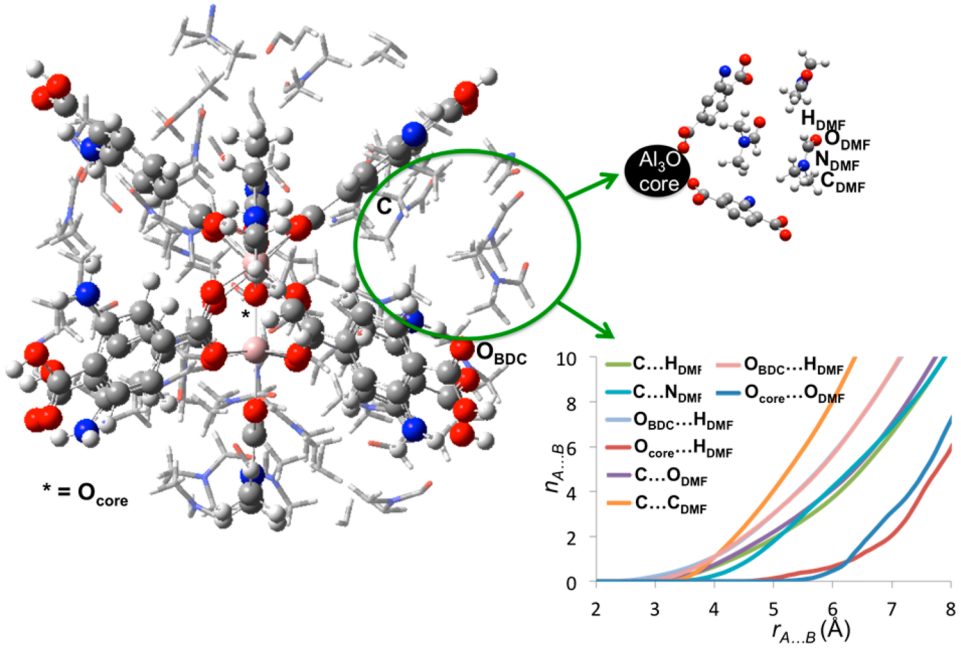

Figure 5. Representative solvent organization (within 12 Å of O_{core}) about $Al_3O(BDC)_6(DMF)_3^+$ in pure DMF. The solvation within the BDC−Al_3O−BDC cleft is inset along with key integrated RDFs between functional groups of $Al_3O(BDC)_6(DMF)_3^+$ and DMF.

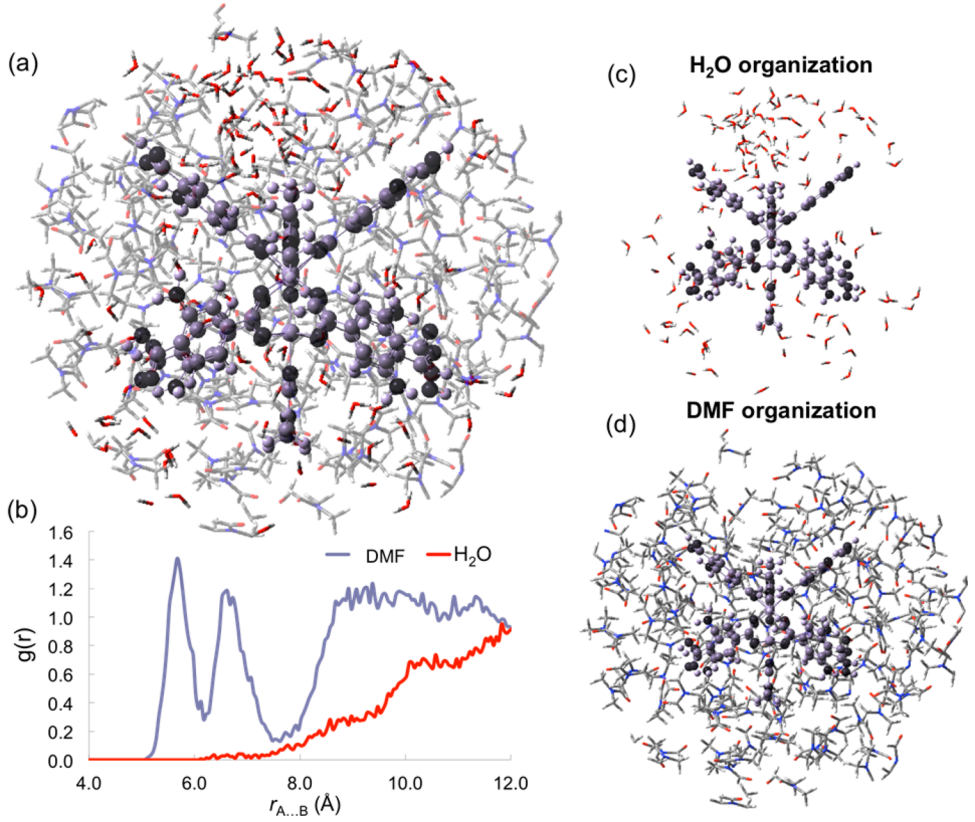

Figure 6. (a) Representative solvent organization (within 18 Å) about $Al_3O(BDC)_6(DMF)_3^+$ in a 1:1 mixture of H_2O/DMF. (b) RDFs between the COM of the cluster and H_2O and DMF molecules, respectively. Contributions of (c) H_2O and (d) DMF solvation.

radial distribution functions (RDFs) between the H and O atoms of H_2O, labeled H_w and O_w, respectively, with the different functional groups associated with the MOF cluster. In general, the solvation shell about the MOF cluster is rather hydrophobic, with the H atoms pointing toward all functional groups and little hydrogen bonding between H_2O and the cluster (Figures 4 and S3 and S4 in the SI). A single hydrogen bond is observed between H_2O and the noncoordinating carbonyl groups of BDC^- (defined by an $O_{BDC}\cdots H_w$ distance of less than 3 Å). Yet this hydrogen-bonding interaction is weak and highly fluxional because it does not serve to organize those H_2O molecules enough to cause a well-resolved peak in the

dx.doi.org/10.1021/ic5006659 | Inorg. Chem. 2014, 53, 8930−8940

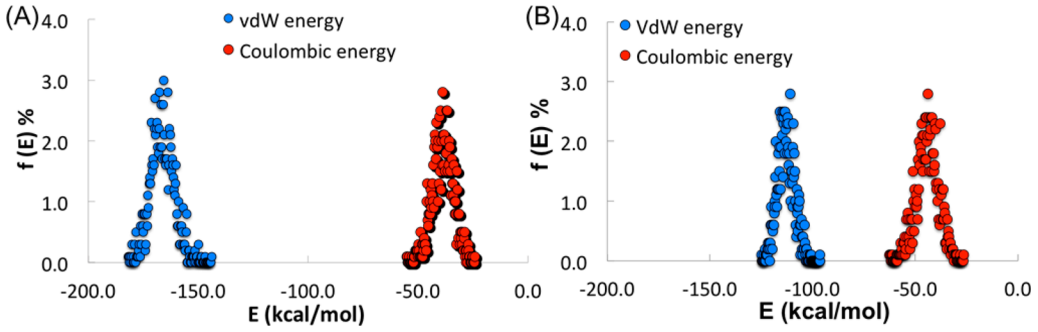

Figure 7. vdW and electrostatic interaction energy distributions within (A) $Al_3O(BDC)_6(DMF)_3^+$ immersed in DMF and (B) $Al_3O(BDC)_6(DMF)_3^+$ immersed in H_2O.

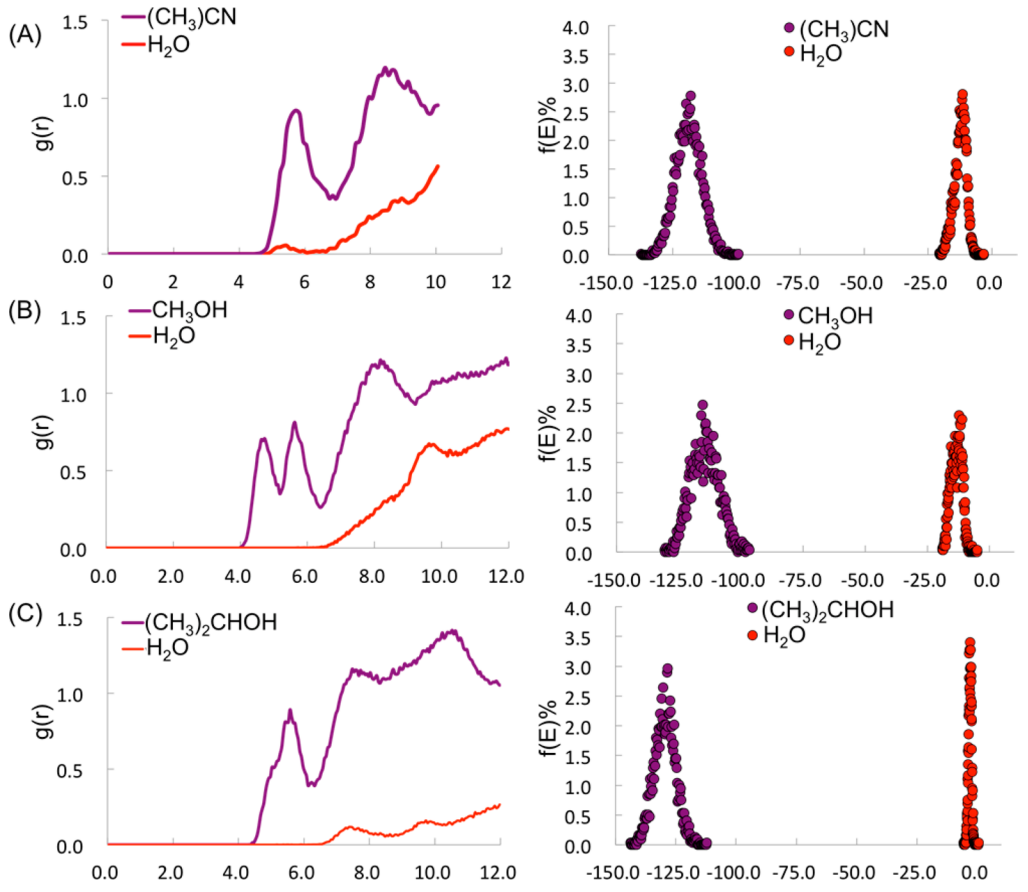

Figure 8. (left-hand panels) RDFs between the COM of the $Al_3O(BDC)_6(DMF)_3^+$ cluster and each solvent. (right-hand panels) Energy distributions for vdW interactions between each solvent and the $Al_3O(BDC)_6(DMF)_3^+$ cluster. The solvent systems presented are (A) a 1:1 solution of $H_2O/(CH_3)CN$, (B) a 1:1 solution of H_2O/MeOH, and (C) a 1:1 solution of $(CH_3)_2CHOH/H_2O$.

RDF. We note that the atomic charges on the terminal carboxylate group (0.15− to 0.27−) are also significantly smaller than the SPC/E charge in the H_2O model (0.83−), which may prevent significant hydrogen bonding between the cluster and H_2O. However, the $-NH_2$ group at the position ortho to the BDC^- carbonyl participates in intramolecular hydrogen bonding with this group, and while this hydrogen bond occurs in the optimized gas-phase geometry of the MOF and is fixed during the simulation, it is likely that within a fully dynamic cluster the intramolecular bond is preferred over potential intermolecular hydrogen bonds with the H_2O solvent because delocalization of the π electrons maintains a planar geometry that facilitates the $-NH_2\cdots OC$ interaction. In general, there is a lack of interaction between the H_2O solvent and the cluster, with the average closest distance between H_2O and the cluster being 4−5 Å. The angle associated with the BDC−Al_3O−BDC connectivity further prevents solvating H_2O from hydrogen bonding to either O_{core} or any of the binding O atoms associated with the DMF or BDC^- groups to the Al, although it does appear that ∼2 H_2O molecules have a long-enough residence time within the cleft of the BDC−Al_3O−BDC region to cause an average organization of those two H_2O molecules, as indicated by the integrated $O_{core}\cdots H_w$ RDF (Figure 4). This lends kinetic feasibility to exchange reactions between coordinating solvent molecules at the Al sites of the Al_3O^{7+} core in addition to the thermodynamic feasibility described above.

dx.doi.org/10.1021/ic5006659 | Inorg. Chem. 2014, 53, 8930−8940

Solvation of $Al_3O(BDC)_6(DMF)_3^+$ immersed in neat DMF was subsequently investigated. While DMF is miscible with H_2O, it may only accept a single hydrogen bond per molecule. Solvation of the MOF cluster by DMF is characterized by many points of hydrophobic contact between the DMF methyl groups and the carbon skeleton of $Al_3O(BDC)_6(DMF)_3^+$. Although there are fewer solvating DMF molecules inside the cleft of the BDC−Al_3O−BDC regions, those existing molecules have their $-CH_3$ groups oriented directly over the BDC^- rings (Figure 5). No hydrogen bonding is found between the noncoordinated carbonyl or −COH groups of BDC^- and the DMF solvent.

The importance and favorability of the hydrophobic interactions between DMF and $Al_3O(BDC)_6(DMF)_3^+$ is clearly manifested within the solvent organization of a 1:1 solution of H_2O/DMF. As can be seen in Figure 6, DMF preferentially solvates the MOF cluster. The RDF between the center of mass (COM) of $Al_3O(BDC)_6(DMF)_3^+$ and the COM of solvating DMF and H_2O molecules (Figure 6b) contains peaks at ∼5.5 and ∼6.5 Å representing organized DMF solvation regions in the BDC−Al_3O−BDC cleft and immediately surrounding BDC^- and the coordinating DMF. In contrast, the RDF between the MOF cluster and H_2O indicates a slow but steady rise in the concentration of solvating H_2O with increased distance. As shown in Figure 6c, a small percentage of H_2O may, at any time, penetrate into the BDC−Al_3O−BDC cleft; however, the density of H_2O and DMF solvent molecules does not become equal until a distance of ∼12 Å from the COM of $Al_3O(BDC)_6(DMF)_3^+$. We further evaluate the solvation structure for the DMF/H_2O mixture at temperatures relevant to hydrothermal synthesis, 370 K. Although the enhanced temperature increases the diffusion coefficients of each solvent (from 1.0 1.0×10^{-9} to 2.9×10^{-9} m^2/s for H_2O and from 0.74 $\times 10^{-9}$ to 2.5×10^{-9} m^2/s for DMF), the preferential solvation of DMF about the cluster is maintained.

The cause of preferential solvation can be understood in terms of the distribution of interaction energy energies between each type of solvent and the MOF cluster. In the neat liquids, both solvents have a fairly weak electrostatic interaction with the monocation MOF cluster (Figure 7). This is because the excess charge is delocalized across the Al_3O^{7+} core and coordinating atoms in both the classical and quantum mechanical descriptions. For both liquids, the dominant contribution to the interaction energy derives from vdW interactions, and as observed in Figure 7, pure DMF has ∼50 kcal/mol more stabilization energy from vdW than H_2O. This is in line with the many points of contact that each DMF molecule can have with the cluster relative to H_2O. For example, a DMF molecule that exists within the BDC−Al_3O−BDC cleft will have more net vdW contributions than a H_2O molecule at the same position.

The extent of preferential solvation for other solvent mixtures that contain hydrophobic functional units was also examined so as to confirm whether this is a general trend that should be considered during MOF synthesis. 1:1 mixtures of H_2O and CH_3CN, $(CH_3)_2CHOH$, and MeOH were examined. While the overall preference for the cosolvent to form a distinct solvation shell about the MOF cluster is maintained, distinct trends in preferential solvation are observed (Figure 8). Ranking the cosolvents based upon their observed ability to exclude H_2O from the MOF cluster yields CH_3CN < DMF ∼ MeOH < $(CH_3)_2CHOH$. Note that this ranking does not correlate well with either the molecular volume of the cosolvent or the previously reported partial molar volumes of aqueous solutions at a mole fraction of 0.5.[57−60] Thus, the molecular solvent−solvent and solvent−solute interactions appear to be the fundamental origin of this behavior. The preferential solvation is anticipated to impact the kinetic aspects of the growth or transformative reactions of the MOF cluster because it should stabilize the topology via its enhanced solute−solvent vdW interactions. Further, these results are likely applicable to the NH_2-MIL-100(Al) intermediate cluster, which has a coordinated OH^- at one of the Al sites in the Al_3O^{7+} core, because the predominant solute−solvent interactions occur on the exterior of the cluster where vdW interactions will be essentially unchanged by the presence of a coordinated OH^- in the center of the cluster.

CONCLUSIONS

A combination of DFT-based cluster calculations and MD simulations has been used to explore key features believed to be important to crystallization of a model MOF crystallite/cluster based upon the metastable phase NH_2-MOF-235(Al). These clusters are of the form $Al_3O(BDC)_6(DMF)_n(H_2O)_m^+$ (n = 1−3; m = {n − 3}). The thermodynamic favorability of coordinated solvent- and ligand-exchange reactions has been studied with the aim of understanding whether or not the coordinated solvent influences the metal−linker binding energy and the sensitivity to the dielectric constant of the solvent medium. The ionic bonding interaction of Al_3O^{7+} with BDC^- (characterized by LOL and bond-order analyses) is found to be much stronger than that with coordinated solvent (H_2O or DMF) and is independent of which solvent is bound to Al_3O^{7+} and also the dielectric constant of the solvent medium. The exchange reactions of coordinated solvent molecules are found to be facile at room temperature, and the solvent organization observed in the MD studies indicates that solvent exchange is kinetically allowed because of the ability of both solvents to migrate into the cleft created by the BDC−Al_3O−BDC coordination angle. This supports the kinetic viability of DMF-promoted reactions that may transform NH_2-MOF-235(Al) into NH_2-MIL-101(Al). Because BDC^- binds to the Al_3O^{7+} core, the solvation free energy (G_{solv}) of the cluster is observed to become less favorable. Within the context of the PCM approach for determining G_{solv}, this arises from a decrease in the stabilizing electrostatic contributions caused by the essentially hydrophobic BDC^- ligand. Thus, as the crystal grows, there is a balance between the energy gained by ligand binding and an increasingly unfavorable free energy of solvation. Ultimately, unfavorable solvation energies will inhibit the formation of quantifiable MOF crystals unless solution-phase conditions can be used to maintain thermodynamically favorable solute−solvent interactions.

The relative hydrophobicity of the $Al_3O(BDC)_6(DMF)_3^+$ cluster is manifested in preferential solvation within binary solutions containing H_2O with either DMF, MeOH, CH_3CN, or $(CH_3)_2CHOH$. Here the relatively hydrophobic cosolvent has a more favorable solute−solvent interaction, leading to the formation of a separate solvation layer near the MOF cluster, with H_2O excluded to far distances from the cluster. The preferential solvation is maintained even at high temperatures analogous to those used in the hydrothermal synthesis of MOFs. While all cosolvents exhibit this preferential solvation, trends do exist. Ranking the cosolvents based upon their observed ability to exclude H_2O from the MOF cluster yields CH_3CN < DMF ∼ MeOH < $(CH_3)_2CHOH$. These

dx.doi.org/10.1021/ic5006659 | Inorg. Chem. 2014, 53, 8930−8940

observations are anticipated to impact the intermediate and final phases observed in MOF synthesis by creating favorable solvation environments for specific MOF topologies. The preferential solvation will presumably act to stabilize the growing cluster and keep it from precipitation longer than if neat H_2O is used because of the enhanced vdW interactions that the relatively hydrophobic cosolvent has with the cluster relative to H_2O. This report suggests that, in addition to any role that DMF may have in the reactive transformation of NH_2-MOF-235(Al) to NH_2-MOF-101(Al), the cosolvent plays a vital role in stabilizing the metastable NH_2-MOF-235(Al) phase early in the synthesis.

■ ASSOCIATED CONTENT

Supporting Information

RDFs and optimized Cartesian coordinates. This material is available free of charge via the Internet at http://pubs.acs.org.

■ AUTHOR INFORMATION

Corresponding Authors

*E-mail: yangxia@njtech.edu.cn..
*E-mail: auclark@wsu.edu

Notes

The authors declare no competing financial interest.

■ ACKNOWLEDGMENTS

Financial support from the U.S. Department of Energy, Office of Basic Energy Sciences, Division of Chemical Sciences, Geosciences, and Biosciences, under Award DE-FG02-12ER16362, is acknowledged. This research was performed using EMSL, a national scientific user facility sponsored by the Department of Energy's Office of Biological and Environmental Research and located at Pacific Northwest National Laboratory.

■ REFERENCES

(1) Long, J. R.; Yaghi, O. M. *Chem. Soc. Rev.* **2009**, *38*, 1213.
(2) Meek, S. T.; Greathouse, J. A.; Allendorf, M. D. *Adv. Mater.* **2011**, *23*, 249−267.
(3) Cook, T. R.; Zheng, Y.-R.; Stang, P. J. *Chem. Rev.* **2013**, *113*, 734−777.
(4) Huang, A.; Dou, W.; Caro, J. *J. Am. Chem. Soc.* **2010**, *132*, 15562.
(5) Finsy, V.; Ma, L.; Alaerts, L.; De Vos, D. E.; Baron, G. V.; Denayer, J. F. M. *Microporous Mesoporous Mater.* **2009**, *120*, 221.
(6) Gu, Z. Y.; Yan, X. P. *Angew. Chem., Int. Ed.* **2010**, *49*, 1477.
(7) Murray, L.; Dinca, M.; Long, J. *Chem. Soc. Rev.* **2009**, *38*, 1294−1314.
(8) Chen, B.; Ockwig, N. W.; Millward, A. R.; Contreas, D. S.; Yaghi, O. M. *Angew. Chem., Int. Ed.* **2005**, *44*, 4745.
(9) Corma, A.; Garcia, H.; Liabres, F. X.; Xamena, I. *Chem. Rev.* **2010**, *110*, 4606.
(10) Gandara, F.; Puebla, E. G.; Lglesias, M.; Proserpio, D. M.; Snejko, N.; Monge, M. A. *Chem. Mater.* **2009**, *21*, 655.
(11) Jiang, D. M.; Urakawa, A.; Yulikov, M.; Mallat, T.; Jeschke, G.; Baiker, A. *Chem.—Eur. J.* **2009**, *15*, 12255.
(12) Taylor, K. M. L.; Jin, A.; Lin, W. *Angew. Chem., Int. Ed.* **2008**, *47*, 7722.
(13) Horcajada, P.; Serre, C.; Vallet-Regi, M.; Sebban, M.; Taulelle, F.; Fercy, G. *Angew. Chem., Int. Ed.* **2006**, *45*, 5974.
(14) Kent, C. A.; Liu, D.; Meyer, T. J.; Liu, W. *J. Am. Chem. Soc.* **2012**, *134*, 3991.
(15) Tran, D. T.; Chernova, N. A.; Chu, D.; Oliver, A. G.; Oliver, S. R. J. *Cryst. Growth Des.* **2010**, *10*, 874.
(16) Ferey, G. *Chem. Soc. Rev.* **2008**, *37*, 191.
(17) Goesten, M.; Stavitski, E.; Pidko, E. A.; Gucuyener, C.; Boshuizen, B.; Ehrlich, S. N.; Hensen, E. J. M.; Kapteijn, F.; Gascon, J. *Chem.—Eur. J.* **2013**, *19*, 7809−7816.
(18) Surble, S.; Millange, F.; Serre, C.; Ferey, G.; Walton, R. I. *Chem. Commun.* **2006**, 1518−1520.
(19) Hermes, S.; Witte, T.; Hikov, T.; Zacher, D.; Bahnmuller, S.; Langstein, G.; Huber, K.; Fischer, R. A. *J. Am. Chem. Soc.* **2007**, *129*, 5324−5325.
(20) Shoaee, M.; Anderson, M. W.; Attfield, M. P. *Angew. Chem., Int. Ed.* **2008**, *47*, 8525−8528.
(21) Khan, N. A.; Jhung, S. H. *Cryst. Growth Des.* **2010**, *10*, 1860−1865.
(22) Haouas, M.; Volkringer, C.; Loiseau, T.; Férey, G.; Taulelle, F. *Chem. Mater.* **2012**, *24*, 2462−2471.
(23) Stativstki, E.; Goesten, M.; Juan-Alcaniz, J.; Martinez-Joaristi, A.; Serra-Crespo, P.; Petukhov, A. V.; Gascon, J.; Kapteijn, F. *Angew. Chem., Int. Ed.* **2011**, *50*, 9624.
(24) Goesten, M. G.; Magusin, P. C. M. M.; Pidko, E. A.; Mezari, B.; Hensen, E. J. M.; Kapteijn, F.; Gascon, J. *Inorg. Chem.* **2014**, *53*, 882−887.
(25) Celic, T. B.; Rangus, M.; Lazar, K.; Kaucic, V.; Logar, N. Z. *Angew. Chem., Int. Ed.* **2012**, *51*, 12490−12494.
(26) Frisch, M. J.; Trucks, G. W.; Schlegel, H. B.; Scuseria, G. E.; Robb, M. A.; Cheeseman, J. R.; Scalmani, G.; Barone, V.; Mennucci, B.; Petersson, G. A.; Nakatsuji, H.; Caricato, M.; Li, X.; Hratchian, H. P.; Izmaylov, A. F.; Bloino, J.; Zheng, G.; Sonnenberg, J. L.; Hada, M.; Ehara, M.; Toyota, K.; Fukuda, R.; Hasegawa, J.; Ishida, M.; Nakajima, T.; Honda, Y.; Kitao, O.; Nakai, H.; Vreven, T.; Montgomery, J. A., Jr.; Peralta, J. E.; Ogliaro, F.; Bearpark, M.; Heyd, J. J.; Brothers, E.; Kudin, K. N.; Staroverov, V. N.; Kobayashi, R.; Normand, J.; Raghavachari, K.; Rendell, A.; Burant, J. C.; Iyengar, S. S.; Tomasi, J.; Cossi, M.; Rega, N.; Millam, M. J.; Klene, M.; Knox, J. E.; Cross, J. B.; Bakken, V.; Adamo, C.; Jaramillo, J.; Gomperts, R.; Stratmann, R. E.; Yazyev, O.; Austin, A. J.; Cammi, R.; Pomelli, C.; Ochterski, J. W.; Martin, R. L.; Morokuma, K.; Zakrzewski, V. G.; Voth, G. A.; Salvador, P.; Dannenberg, J. J.; Dapprich, S.; Daniels, A. D.; Farkas, Ö.; Foresman, J. B.; Ortiz, J. V.; Cioslowski, J.; Fox, D. J. *Gaussian 09*, revision D.01; Gaussian, Inc.: Wallingford, CT, 2009. Becke, A. D. *J. Chem. Phys.* **1993**, *98*, 5648−5652.
(27) Lee, C.; Yang, W.; Parr, R. G. *Phys. Rev. B* **1988**, *37*, 785−789.
(28) Dunning, T. H., Jr. *J. Chem. Phys.* **1989**, *90*, 1007−1023.
(29) Woon, D. E.; Dunning, T. H., Jr. *J. Chem. Phys.* **1993**, *98*, 1358−1371.
(30) Boys, S. F.; Bernardi, F. *Mol. Phys.* **1970**, *19*, 553.
(31) Lu, T. *Multiwfn*, version 1.4; http://multiwfn.codeplex.com/.
(32) Mayer, I. *Int. J. Quantum Chem.* **1984**, *26*, 151−154.
(33) Foster, J. P.; Weinhold, F. *J. Am. Chem. Soc.* **1980**, *102*, 7211−7218.
(34) Reed, A. E.; Curtiss, L. A.; Weinhold, F. *Chem. Rev.* **1988**, *88*, 899−926.
(35) Marenich, A. V.; Cramer, C. J.; Truhlar, D. G. *J. Phys. Chem. B* **2009**, *113*, 6378−6396.
(36) http://www.ccp5.ac.uk/DLPOLYCLASSIC/.
(37) http://www.ime.unicamp.br/~martinez/packmol.
(38) Mayo, S. L.; Olafson, B. D.; Goddard, W. A., III. *J. Phys. Chem.* **1990**, *94*, 8897−8909.
(39) Berendsen, H. J. C.; Grigera, J. R.; Straatsma, T. P. *J. Phys. Chem.* **1987**, *91*, 6269.
(40) Price, M. L. P.; Ostrovsky, D.; Jorgensen, W. L. *J. Comput. Chem.* **2001**, *22*, 1340−1352.
(41) Jorgensen, W. L.; Maxwell, D. S.; Tirado-Rives, J. *J. Am. Chem. Soc.* **1996**, *118*, 11225−11236.
(42) Lei, Y.; Li, H.; Pan, H.; Han, S. *J. Phys. Chem. A* **2003**, *107*, 1574−1583.
(43) Wick, C. D.; Stubbs, J. M.; Rai, N.; Siepmann, I. I. *J. Phys. Chem. B* **2005**, *109*, 18974−18982.
(44) Chen, B.; Potoff, J. J.; Siepmann, J. I. *J. Phys. Chem. B* **2001**, *105*, 3093−3104.

(45) Melchionna, S.; Ciccotti, G.; Hollan, B. L. *Mol. Phys.* **1993**, *78*, 533−544.
(46) Martyna, G. J.; Tobias, D. J.; Klein, M. L. *J. Chem. Phys.* **1994**, *101*, 4177−4189.
(47) Nosé, S. *J. Chem. Phys.* **1984**, *81*, 511−519.
(48) Hoover, W. G. *Phys. Rev. A* **1985**, *31*, 1695−1697.
(49) Thijssen, J. M. *Computational Physics*, 2nd ed.; Cambridge University Press: Cambridge, U.K., 2007; pp 226−231.
(50) Swope, W. C.; Anderson, H. C. *J. Phys. Chem.* **1984**, *88*, 6548−6556.
(51) Sudik, A. C.; Cote, A. P.; Yaghi, O. M. *Inorg. Chem.* **2005**, *44*, 2998−3000.
(52) Greathouse, J. A.; Allendorf, M. D. *J. Am. Chem. Soc.* **2006**, *128*, 10678−10679.
(53) Zhao, Y.; Truhlar, D. G. *J. Chem. Phys.* **2006**, *125*, 194101.
(54) Zhao, Y.; Truhlar, D. G. *Acc. Chem. Res.* **2008**, *41*, 157.
(55) Schmider, H. L.; Becker, A. D. *THEOCHEM* **2000**, *527*, 51−61.
(56) Gostern, M. G.; Staviski, E.; Juan-Alcaniz, J.; Martinez-Joaristi, A.; Petukhov, A. V.; Kapteijn, F.; Gascon, J. *Catal. Today* **2013**, *205*, 120−127.
(57) Bai, T.-C.; Yao, J.; Han, S.-J. *J. Chem. Eng. Data* **1999**, *44*, 491−496.
(58) Sakurai, M. *J. Chem. Eng. Data* **1992**, *37*, 358−362.
(59) Sakurai, M. *J. Solution Chem.* **1988**, *17*, 267−275.
(60) Hyncica, P.; Hnedkovsky, L.; Cibulka, I. *J. Chem. Thermodyn.* **2004**, *36*, 1095−1103.